Using sedimentological priors to improve ^{14}C calibration of bioturbated sediment archives.

Bryan C. Lougheed
Department of Earth Sciences, Uppsala University, Sweden
bryan.lougheed@geo.uu.se

Abstract

Radiocarbon (^{14}C) dating is often carried out upon multi-specimen samples sourced from bioturbated sediment archives, such as deep-sea sediment. These samples are inherently heterogeneous in age, but current ^{14}C calibration techniques applied to such age heterogenous samples were originally developed for age homogeneous material. A lack of information about age heterogeneity leads to a systematic underestimation of a sample's true age range, as well as the possible generation of significant age-depth artefacts during periods of highly dynamic $\Delta^{14}C$. Here, a calibration protocol is described that allows for the application of sedimentological priors describing sediment accumulation rate, bioturbation depth and temporally dynamic species abundance. This Bayesian approach produces a credible calibrated age distribution associated with a particular laboratory ^{14}C determination and its associated sedimentological priors, resulting in an improved calibration, especially in the case of low sediment accumulation rates typical of deep-sea sediment. A time-optimised computer script (*biocal*) for the new calibration protocol is also presented, thus allowing for rapid and automated application of the new calibration protocol using sedimentological priors. This new calibration protocol can be applied within existing age-depth modelling software packages to produce more accurate geochronologies for bioturbated sediment archives.

1.0 Introduction

Radiocarbon (^{14}C) analysis is routinely used to determine the age of marine sediment archives, and has been fundamental in increasing understanding the spatio-temporal development of global ocean and geochemical parameters during the last glacial and the Holocene. However, due to ^{14}C being a very rare radioisotope in the environment (approximately one in one trillion carbon dioxide molecules in the atmosphere is $^{14}CO_2$), it is more difficult to measure than more common, stable carbon isotopes. From a practical standpoint, this rarity results in a requirement of relatively large

sample sizes to attain a sufficient measurement signal using, e.g., accelerated mass spectrometry (AMS). In the case of, e.g., deep-sea sediment archives, many tens of single microfossil specimens are often pooled into a single sample for measurement.

Systematic bioturbation of deep-sea sediment causes discrete downcore intervals of deep-sea sediment to have an age distribution that is characterised by an exponential probability density function with a long tail towards older ages (Berger and Heath 1968). This age distribution is mainly governed by the sediment accumulation rate (SAR) and bioturbation depth (BD), the latter of which is typically around 10 cm (Trauth et al. 1997; Boudreau 1998). The presence of the aforementioned age distribution is supported by studies of, e.g., particle mixing, stable isotopes, ^{14}C, species abundance and tephras (Bramlette and Bradley 1942; Nayudu 1964; Ruddiman and Glover 1972; Peng et al. 1979; Hutson 1980; Pisias 1983; Schiffelbein 1984; Andree 1987; Bard et al. 1987; Wheatcroft 1992; Trauth et al. 1997; Henderiks et al. 2002; Löwemark and Grootes 2004; Sepulcre et al. 2017; Lougheed et al. 2018; Abbott et al. 2018; Missiaen et al. 2020; Dolman et al. 2020).

Following (Berger and Heath 1968), the 1σ age value of a 1 cm slice of a sediment archive with a sediment accumulation rate of 5 cm ka^{-1} and a bioturbation depth of 10 cm can be approximated as $10/5 \times 1000 = 2000$ yr. Somewhat counter-intuitively, that same sediment archive will exhibit a downcore increasing mean age of $1000/5 = 200$ yr cm^{-1}, which has led many researchers to incorrectly assume that multi-specimen samples retrieved from such a sediment archive represent a downcore temporal resolution of 200 yr cm^{-1}. However, downcore increase in mean age is not the same concept as the temporal resolution of multi-specimen samples retrieved from the archive.

The current state of the art in palaeoclimate includes no information about bioturbation when ^{14}C calibrating multi-specimen samples retrieved from deep-sea sediment (or lacustrine) archives. In essence, the current state of the art considers only the ^{14}C-centric uncertainties when estimating (calibrating) true age, i.e. those uncertainties relating to the laboratory measurement, calibration curve and ^{14}C reservoir effect. Such an approach incorrectly considers deep-sea sediment as having discrete age increments, i.e. similar to non-bioturbated archives such as tree rings, speleothems and/or varves. The current lack of method for considering bioturbation when applying the ^{14}C method to deep-sea sediment can lead to an underestimation of the full age uncertainty. Furthermore, not considering the effect of bioturbation upon the age distribution of single

microfossils within a sediment archive results in a systematically incorrect calibration, which can lead to the production of age-depth artefacts (Lougheed et al. 2020). These artefacts are further amplified for sediment intervals coinciding with highly dynamic $\Delta^{14}C$ and/or $\Delta^{14}C$ plateaus (*ibid.*). Such age-depth artefacts could potentially be misidentified as true age-depth features in the sediment, and incorrectly attributed to, e.g., environmental and/or climatological processes.

2.0 Method

The calibration process presented here involves using quantitative priors for sediment accumulation rate, bioturbation depth and temporal changes in species abundance to estimate the credible age distribution for a sample that would result in the observed ^{14}C activity determination derived from a given sample. In addition to the prescribed priors, this process must also take into account all ^{14}C uncertainties, i.e uncertainties pertaining the laboratory determination, past $\Delta^{14}C$ (the calibration curve) and reservoir effect. To avoid ambiguity, throughout this text the use of the term "age" refers exclusively to true/calibrated age, while ^{14}C activity is always referred to as ^{14}C activity, i.e. not as "^{14}C age".

2.1 Establishing a prior distribution for calendar age

In order to calibrate ^{14}C activity measurements carried out upon heterogeneous samples retrieved from bioturbated sediment, the following sedimentological priors are defined:

s = estimated sediment accumulation rate (SAR), in cm yr^{-1}
m = bioturbation (mixing) depth (BD), in cm.
k = the fraction of the analysed microfossils that are fragmented (a value between 0 and 1)
a = time series of abundance of the analysed species relative to itself (values between 0 and 1)

Both SAR and BD are considered here as a single value, i.e. not as a time series of temporally variable values. These parameters are kept static foremost to reduce computation time, and also because temporal changes in, e.g., SAR (the relationship between mean age and depth) are not known when an age-depth chronology has yet to be developed. In short, applying detailed information about temporal changes in SAR when the age of the sediment is not yet known would constitute circular thinking.

The sedimentological priors can be used to construct a prior distribution of relative age for the sample being calibrated. Following (Berger and Heath 1968), the age distribution for a given depth of fully bioturbated sediment core can be represented by an exponential probability distribution, which can be considered the basis of the prior probability distribution for our sample's calibrated age:

$$p_{prior}(r_1, r_2, \ldots, r_n) = \exp\left(\frac{-(r_1, r_2, \ldots, r_n)s}{m}\right) \quad \text{(Eq. 1)}$$

where r is the relative age (starting at 1 yr) within P_{prior}. The low-probability long tail of an exponential probability function continues to infinity, which obviously cannot be stored in computer memory. The prior distribution is therefore limited to the age equivalent value of five bioturbation depths, i.e. a relative age of $r_{limit} = 5m / s$, which is rounded to the nearest whole year.

When picking microfossils for ^{14}C analysis, palaeoceanographers generally prefer to pick whole specimens. The fragmented and/or dissolved microfossils that are not picked have been exposed to more bioturbation samples, and as such represent the oldest fraction of the sample (Rubin and Suess 1955; Ericson et al. 1956; Emiliani and Milliman 1966; Barker et al. 2007). Information regarding this effect should be incorporated into the prior distribution. The fraction of fragmented microfossils (k) can be related to the cumulative expression of Eq. 1 as follows:

$$1 - k = 1 - \exp\left(\frac{-r\,s}{m}\right) \quad \text{(Eq. 2)}$$

Eq. 2 can be solved to attain $r(k)$, the threshold age for fragmented foraminifera:

$$r(k) = \frac{-m \ln(k)}{s} \quad \text{(Eq. 3)}$$

Regions of the prior probability distribution (p_{prior}) older than $r(k)$ can, therefore, be considered to consist of fragmented microfossils that are not picked by palaeoceanographers. When $r(k) < r_{limit}$, p_{prior} is truncated at the discrete relative age $r(k)$ to incorporate prior information from the picking

process. When r(k) ≥ r_{limit}, *r(k)* is approximated to r_{limit}. All discrete probability values in p_{prior} are subsequently normalised such that they sum to 1.

2.2 Establishing a distribution for ^{14}C activity

The calibration process carried out must incorporate the full uncertainty regarding ^{14}C activity, which includes uncertainties regarding the laboratory ^{14}C activity determination, the calibration curve ^{14}C activity, and the ^{14}C activity depletion as a result of the reservoir effect. These are expressed here as follows:

A_{det} = The laboratory ^{14}C activity determination of the sample (in ^{14}C yr BP) .
σ_{det} = The measurement uncertainty associated with A_{det} (in ^{14}C yr).

$A_{cc}(t)$ = The ^{14}C activity (in ^{14}C yr BP) predicted by the calibration curve for a discrete age *t*.
$\sigma_{cc}(t)$ = The uncertainty (in ^{14}C yr) associated with $A_{cc}(t)$.

R(t) = The predicted ^{14}C activity depletion (in ^{14}C yr) of A_{det} relative to the calibration curve at discrete age *t*, due to a local reservoir effect (Stuiver et al. 1986). *R(t)* can be substituted with *ΔR(t)* in the case of a marine calibration curve.
$\sigma_R(t)$ = The uncertainty (in ^{14}C yr) associated with *R(t)* (or *ΔR(t)*).

Activity depletion due to *R(t)* is considered here by incorporating it into the calibration curve ^{14}C activity. This approach to handling *R(t)* allows, if desired, for temporally dynamic *R(t)* to be correctly incorporated (Waelbroeck et al. 2019). The calibration curve is adjusted as follows, for each discrete calendar age *t*:

$$A_{ccR}(t) = A_{cc}(t) + R(t) \quad \text{(Eq. 4)}$$

Uncertainties pertaining to calibration curve ^{14}C activity and the ^{14}C reservoir effect ($\sigma_{cc}(t)$ and $\sigma_R(t)$) are both Gaussian, so they can be easily propagated into one term, for each discrete calendar age *t*:

$$\sigma_{ccR}(t) = \sqrt{(\sigma_{cc}^2(t) + \sigma_R^2(t))} \quad \text{(Eq. 5)}$$

Before proceeding, all of the above ^{14}C-related parameters are first converted into F^{14}C space to facilitate more accurate calculations that take isotope mass balance into account, which is especially relevant in the case of wide range of ^{14}C activity (Erlenkeuser 1980; Bronk Ramsey 2008; Keigwin and Guilderson 2009), such as is the case with bioturbated sediment archives.

A sequence of probabilities can describe the closeness of a sequence of ^{14}C activities predicted for all discrete ages t (represented as T) available within the calibration curve (i.e. $A_{ccR}(T)$), to a single ^{14}C activity predicted by the calibration curve for a discrete age t (i.e. $A_{ccR}(t)$). This closeness, which includes a quantification of calibration curve and reservoir effect uncertainties, can be evaluated using a normal distribution for each instance of t, summing through all n values available in T to give the total relative ^{14}C probability for each t:

$$p_{14C}(T|t)=\sum_{T_1}^{T_n}\left(\frac{1}{\sigma_{ccR}(t)\sqrt{(2\pi)}}\exp\left(\frac{-(A_{ccR}(T)-A_{ccR}(t))^2}{2\,\sigma_{ccR}^2(t)}\right)\right) \quad \text{(Eq. 6)}$$

2.3 The prior calibration process

The prior calibration process involves moving the p_{prior} distribution along a sliding window of calendar ages and each time computing the the hypothetical laboratory mean ^{14}C activity determination (h_{det}) that would result from each p_{prior} placed at a sliding window starting at each t:

$$h_{det}(t)=\sum_{r=1}^{r(k)}\left(A_{ccR}(t+r-1)\cdot p_{14C}(T|t+r-1)\cdot p_{prior}(r)\cdot a(t+r-1)\right) \quad \text{(Eq. 7)}$$

Subsequently, it is possible to evaluate the single probability value of each $h_{det}(t)$ as a function of its closeness to the normal distribution of the sample's observed laboratory determination $A_{det} \pm \sigma_{det}$:

$$p_{h_{det}}(t)=\frac{1}{\sigma_{det}(t)\sqrt{(2\pi)}}\exp\left(\frac{-(h_{det}(t)-A_{det})^2}{2\,\sigma_{det}^2}\right) \quad \text{(Eq. 8)}$$

For each sliding window placed at each t, a vector of calibrated age probabilities is calculated, corresponding to each discrete age in the sliding window:

$$p_{cal}(t) = p_{h_{det}}(t) \cdot \left(p_{prior}(r, r+1, \ldots, r(k)) \odot a(t, t+1, \ldots, t+r(k)-1) \right) \quad \text{(Eq. 9)}$$

Subsequently, each $p_{cal}(t)$ is sorted into a large matrix, referred to here as $M_{cal}(T)$:

$$M_{cal}(T) = \begin{bmatrix} p_{cal}(t_1)_1 & p_{cal}(t_1)_2 & \ldots & p_{cal}(t_1)_n & 0 & 0 \\ 0 & p_{cal}(t_2)_1 & p_{cal}(t_2)_2 & \ldots & p_{cal}(t_2)_n & 0 \\ 0 & \ddots & \ddots & \ddots & \ddots & 0 \\ 0 & 0 & p_{cal}(t_n)_1 & p_{cal}(t_n)_2 & \ldots & p_{cal}(t_n)_n \end{bmatrix}$$

(Eq. 10)

The final credible calibrated probability distribution corresponding to all ages T can be calculated simply by summing all rows in $M_{cal}(T)$:

$$p_{cal}(T) = \sum_{i=1}^{n} M_{cal}(T)_{ij} \quad \text{(Eq. 11)}$$

All elements in the resulting vector $p_{cal}(T)$ are subsequently normalised such that they sum to 1.

2.4 Script for automated calibration (*biocal)*

Here, a fully documented Matlab function (*biocal.m*) is provided for automated calculation of the procedures outlined in this study, with full compatibility in Octave. Other programming language versions of the script (e.g. Python, Julia and R) are forthcoming and will be uploaded to the same software repository upon completion. The *biocal* script takes full advantage of computer memory to carry out calculations using vectorised programming, thus resulting in a time-optimised routine. In the calibration protocol described here, it is assumed that it is possible to calculate P_{prior} sliding windows along the the entire history covered by the calibration curve. However, as it would be computationally prohibitive to calibrate for the entire history of the calibration curve, *biocal* restricts its P_{prior} sliding window calculations to an interval of the calibration curve covering a 3σ distance in each direction from the laboratory ^{14}C determination, with added padding to accommodate a long tail of P_{prior} sitting at 3σ sigma distance. In future, when computer memory and

processor power increases by another order of magnitude, it will be possible to compute sliding windows across the entire calibration curve, assuming that would ever be deemed necessary. The calculation time and memory usage is inversely related to the SAR, BD, ^{14}C measurement error, calibration curve uncertainty and reservoir effect uncertainty. Testing using Matlab 2020a on a Linux system with an Intel i7-9700 CPU resulted in the following times and memory usage: a Younger Dryas aged sample with SAR of 4 cm ka^{-1} and BD of 10 cm required 1.7 s calculation time and 2GB memory; the same sample, but with a SAR of 20 cm/ka^{-1}, required 0.2 s to calculate and used 100 MB of memory.

3.0 Ground-truth evaluation

3.1 Evaluating calibration using sedimentological priors

Here, a test is carried out to determine if a the calibration protocol incorporating sediment priors results in an improved calibration process (i.e. a better estimation of the true age distribution of the measured sample) for a number of SAR scenarios using a globally representative BD of 10 cm. First, the established understanding of bioturbation (Berger and Heath 1968) is used to calculate the associated annualised age distribution that would be expected for a discrete-depth, 1 cm sediment sample (Fig. 1). In all cases, the mean value of the age distribution is set at 12 ka, and it is assumed that the oldest 10% of the foraminifera are broken, not picked and, therefore, not included in the distribution. This age distribution represents the ground-truth age distribution of our virtual sample, the target age distribution which would be the ideal calibrated age result. Subsequently, we can carry out a 'virtual AMS analysis' upon the ground-truth distribution by using the *IntCal20* (Reimer et al. 2020) calibration curve to determine the mean ^{14}C activity that could be expected, in a best-case scenario, to result from the aforementioned age distribution. For simplicity's sake, no reservoir effect is included in this demonstration, and it is assumed that the mean ^{14}C activity reported by *IntCal20* perfectly represents the ^{14}C activity recorded by the sediment archive, with linear interpolation applied where necessary to achieve annual resolution.

Assuming an appropriate AMS machine error of ±80 ^{14}C yr, the mean ^{14}C activity can then be calibrated in two ways, which can subsequently be compared: **(1)** using *IntCal20* and *Matcal 3.1* (Lougheed and Obrochta 2016) to carry out the existing, standard ^{14}C calibration procedure following, e.g., (Bronk Ramsey 2008); **(2)** using the aforementioned *biocal* in combination with

IntCal20, supplemented by the SAR and BD priors associated with each scenario, to carry out the new calibration protocol outlined in this study.

As could be expected, the calibration protocol using sedimentological priors outperforms the standard calibration procedure in estimating the ground-truth age distribution, as shown in Fig. 1 for a number of SAR scenarios ranging between 4 and 20 cm/ka, with BD of 10 cm and constant temporal species abundance. In such use case scenarios, using the calibration protocol with sedimentological priors demonstrably leads to a more accurate calibrated age distribution, which would be ideal for improving age-depth modelling routines.

In Fig. 2, the SAR scenarios from Fig. 1 are repeated in the case of a much older ground-truth scenario (mean age of 32 ka), whereby Gaussian uncertainties associated with both the sample ^{14}C activity (±300 ^{14}C yr assumed here) and the ^{14}C calibration curve are markedly increased. In Figs. 2e,f,g,h,i it can be seen that these larger uncertainties, when combined with increasing SAR, lead to the sedimentological priors becoming overwhelmed by the Gaussian ^{14}C uncertainties and, consequently, the calibrated age distribution determined by the procedure starts to approach a normal distribution. In these use case scenarios, the calibration protocol using sedimentological priors does not necessarily offer any advantage over the traditional calibration method.

3.3 Evaluating calibration using sedimentological and abundance priors

Temporal changes in species abundance (e.g. of foraminifera) will affect the shape of the species' age distribution for a given discrete depth. Here, a sine wave with a wavelength of 2000 years is used, purely for demonstrational purposes, as a theoretical temporal abundance function (Fig. 3). In Fig. 4, the same SAR scenarios as in Fig. 1 are analysed, but this time with the application of the abundance aspect. Firstly, the aforementioned sinusoidal temporal abundance function is applied to the ground truth distribution. Subsequently, the same abundance function is used as an additional prior input when running *biocal*, to complement the sedimentological priors. The results in Fig. 4 demonstrate how known information about temporal changes in species abundance can be used to produce better informed calibrated age estimations for bioturbated sediment archives. In Fig. 5, the 2000 year wavelength abundance function is also applied to in the case of an older ground-truth distribution (i.e. that of Fig. 3), demonstrating that abundance priors can also be used as a tool to better constrain ^{14}C analysis of older samples with greater uncertainty.

4.0 Advice for determining prior values

In order to carry out the calibration protocol detailed here, prior values for SAR, BD, fraction broken foraminifera, temporal species abundance and temporal reservoir effect are required. A first order estimate for the sediment accumulation rate can be ascertained by examining the general relationship between age-depth determinations (including ^{14}C-derived age estimates based on existing calibration methods without sedimentological priors). It is possible to use an approximate prior for bioturbation depth using an estimate based on globally representative values (generally between 8 and 12 cm) (Trauth et al. 1997; Boudreau 1998). One could also directly estimate for the sediment archive itself based on ^{14}C investigations of the core top (Peng et al. 1979; Trauth et al. 1997; Henderiks et al. 2002), or by using ^{14}C measurements on single foraminifera (Lougheed et al. 2018) or, more accessibly, by measuring ^{14}C on a number of samples with low numbers of foraminifera and using a statistical analysis of the sample variation to infer downcore bioturbation depth (Dolman et al. 2020).

The fraction of unpicked, fragmented microfossils can be estimated by simply investigating the sample material (Le and Shackleton 1992). There is a risk, however, that the very oldest microfossils of the original population are completely dissolved and are therefore no longer present in the sample material as broken material (Ruddiman and Heezen 1967), which could affect assumptions regarding the p_{prior} age distribution. In any case, one can take into account the susceptibility of a particular species to breakage (Boltovskoy 1991; Boltovskoy and Totah 1992) in combination with knowledge of bottom water chemistry (Ruddiman and Heezen 1967; Parker and Berger 1971), as well as the average residence time in the bioturbation zone, itself a function of SAR and BD (Lougheed et al. 2020).

Additional challenges are associated with determining temporal changes in species abundance, seeing as the abundance record sourced from the depth domain (i.e. the downcore, discrete-depth record) is itself modified by bioturbation (Lougheed 2020), and therefore does not reflect the original species abundance signal in the time domain. Species abundance in the time domain, which is called for in the calibration protocol outlined here, could be based on an estimates from, e.g., a transient palaeoclimate model run linked to an ecological model (Lombard et al. 2011; Morard et al. 2013; Roche et al. 2018; Metcalfe et al. 2020), although estimating relative temporal abundance of a

species using such an approach remains a challenging task. Temporal reconstructions of abundance represent an inherent difficulty for the interpretation not just of ^{14}C chronological data, but downcore, multi-specimen microfossil records in general (Bard 2001; Löwemark and Grootes 2004; Löwemark et al. 2008; Lougheed 2020). A suitable approach could involve applying multiple plausible abundance scenarios when calibrating ^{14}C dates using the calibration protocol outlined here, and examining if the spread of calibrated age outcomes significantly affects the geochronological interpretation.

5.0 Conclusion

Current ^{14}C calibration routines for sediment archives do not incorporate information about sedimentological processes such as SAR and BD, meaning that current ^{14}C-based geochronologies systematically underestimate the total age range of a multi-specimen sample, and potentially also contain age-depth artefacts. By taking account of sedimentological processes in addition to ^{14}C uncertainties, a more credible calibrated age distribution can be ascertained using the protocol outlined here. It should be noted that this new calibration protocol offers most improvement in the case of lower SAR typical of deep-sea sediment archives. Determining complex, time-dependent variables such as species abundance is a complex task, and end users are encouraged to experiment with multiple, plausible abundance scenarios determine how they may affect the geochronological interpretation of their data. Similarly, it is possible to experiment with a range of plausible SAR and BD values. Gaining insight into uncertainties through this type of experimentation is important, because SAR itself can influence the age distribution (and hence ^{14}C activity distribution) of a sample, but in order to determine SAR accurately one needs to know the age of the sediment. This *Catch-22* type situation inherently limits high-temporal resolution geochronological analysis of deep-sea sediment, so an experimental approach involving a range of plausible scenarios can help assign suitable uncertainty. Such an approach can be facilitated by the computerised implementation (*biocal*) of the calibration protocol presented here, allowing for many scenarios to be rapidly explored. This time-efficient, vectorised computer script could be ported to and included in existing geochronological software packages typically applied to sediment archives (Bronk Ramsey 1995; Haslett and Parnell 2008; Parnell et al. 2008; Blaauw 2010; Blaauw and Christen 2011; Lougheed and Obrochta 2019), thus leading to improved age-depth chronologies, and ultimately improving the accuracy of geochronological interpretation of sediment archives.

Acknowledgements

The author acknowledges Swedish Research Council (Vetenskapsrådet – VR) *Starting Grant* number 2018-04992.

Software availability

The latest version of *biocal* can be downloaded from https://github.com/bryanlougheed/biocal/ and release versions are archived at *[doi link to permanent repository at Zenodo upon publication]*

References

Abbott PM, Griggs AJ, Bourne AJ, Davies SM. 2018. Tracing marine cryptotephras in the North Atlantic during the last glacial period: Protocols for identification, characterisation and evaluating depositional controls. Marine Geology. 401:81–97. https://doi.org/10.1016/j.margeo.2018.04.008

Andree M. 1987. The Impact of Bioturbation on AMS 14C Dates On Handpicked Foraminifera: A Statistical Model. Radiocarbon. 29(2):169–175. https://doi.org/10.1017/S0033822200056927

Bard E. 2001. Paleoceanographic implications of the difference in deep-sea sediment mixing between large and fine particles. Paleoceanography. 16(3):235–239.

Bard E, Arnold M, Duprat J, Moyes J, Duplessy JC. 1987. Reconstruction of the last deglaciation: Deconvolved records of δ 18 O profiles, micropaleontological variations and accelerator mass spectrometric 14 C dating. Climate Dynamics. 1(2):101–112.

Barker S, Broecker W, Clark E, Hajdas I. 2007. Radiocarbon age offsets of foraminifera resulting from differential dissolution and fragmentation within the sedimentary bioturbated zone. Paleoceanography. 22(2):PA2205. https://doi.org/10.1029/2006PA001354

Berger WH, Heath GR. 1968. Vertical mixing in pelagic sediments. Journal of Marine Research. 26:134–143.

Blaauw M. 2010. Methods and code for 'classical' age-modelling of radiocarbon sequences. Quaternary Geochronology. 5(5):512–518.

Blaauw M, Christen JA. 2011. Flexible Paleoclimate Age-Depth Models Using an Autoregressive Gamma Process. Bayesian Analysis. 6:457–474. https://doi.org/10.1214/11-BA618

Boltovskoy E. 1991. On the destruction of foraminiferal tests (laboratory experiments). Révue de Micropaléontologie. 34(1):p12-25.

Boltovskoy E, Totah V. 1992. Preservation index and preservation potential of some foraminiferal species. Journal of Foraminiferal Research. 22(3):267–273. https://doi.org/10.2113/gsjfr.22.3.267

Boudreau BP. 1998. Mean mixed depth of sediments: The wherefore and the why. Limnology and Oceanography. 43(3):524–526. https://doi.org/10.4319/lo.1998.43.3.0524

Bramlette M, Bradley W. 1942. Geology and biology of North Atlantic deep-sea cores. Part 1. Lithology and geologic interpretations. Prof Pap US Geol Surv. 196 A:1–34.

Bronk Ramsey C. 1995. Radiocarbon calibration and analysis of stratigraphy; the OxCal program. Radiocarbon. 37(2):425–430.

Bronk Ramsey C. 2008. Radiocarbon dating: Revolutions in Understanding. Archaeometry. 50(2):249–275.

Dolman AM, Groeneveld J, Mollenhauer G, Ho SL, Laepple T. 2020. Estimating bioturbation from replicated small-sample radiocarbon ages. Earth and Space Science Open Archive [Internet]. [accessed 2020 Oct 27]. https://doi.org/10.1002/essoar.10504501.2

Emiliani C, Milliman JD. 1966. Deep-sea sediments and their geological record. Earth-Science Reviews. 1(2–3):105–132. https://doi.org/10.1016/0012-8252(66)90002-X

Ericson DB, Broecker WS, Kulp JL, Wollin G. 1956. Late-Pleistocene Climates and Deep-Sea Sediments. Science. 124(3218):385–389. https://doi.org/10.1126/science.124.3218.385

Erlenkeuser H. 1980. 14C age and vertical mixing of deep-sea sediments. Earth and Planetary Science Letters. 47(3):319–326. https://doi.org/10.1016/0012-821X(80)90018-7

Haslett J, Parnell A. 2008. A simple monotone process with application to radiocarbon-dated depth chronologies. Journal of the Royal Statistical Society: Series C (Applied Statistics). 57(4):399–418. https://doi.org/10.1111/j.1467-9876.2008.00623.x

Henderiks J, Freudenthal T, Meggers H, Nave S, Abrantes F, Bollmann J, Thierstein HR. 2002. Glacial–interglacial variability of particle accumulation in the Canary Basin: a time-slice approach.

Deep Sea Research Part II: Topical Studies in Oceanography. 49(17):3675–3705. https://doi.org/10.1016/S0967-0645(02)00102-9

Hutson WH. 1980. Bioturbation of deep-sea sediments: Oxygen isotopes and stratigraphic uncertainty. Geology. 8(3):127–130. https://doi.org/10.1130/0091-7613(1980)8<127:BODSOI>2.0.CO;2

Keigwin LD, Guilderson TP. 2009. Bioturbation artifacts in zero-age sediments. Paleoceanography. 24(4):PA4212. https://doi.org/10.1029/2008PA001727

Le J, Shackleton NJ. 1992. Carbonate Dissolution Fluctuations in the Western Equatorial Pacific During the Late Quaternary. Paleoceanography. 7(1):21–42. https://doi.org/10.1029/91PA02854

Lombard F, Labeyrie L, Michel E, Bopp L, Cortijo E, Retailleau S, Howa H, Jorissen F. 2011. Modelling planktic foraminifer growth and distribution using an ecophysiological multi-species approach. Biogeosciences. 8(4):853–873. https://doi.org/10.5194/bg-8-853-2011

Lougheed BC. 2020. SEAMUS (v1.20): a Δ14C-enabled, single-specimen sediment accumulation simulator. Geoscientific Model Development. 13(1):155–168. https://doi.org/10.5194/gmd-13-155-2020

Lougheed BC, Ascough P, Dolman AM, Löwemark L, Metcalfe B. 2020. Re-evaluating 14C dating accuracy in deep-sea sediment archives. Geochronology. 2(1):17–31. https://doi.org/10.5194/gchron-2-17-2020

Lougheed BC, Metcalfe B, Ninnemann US, Wacker L. 2018. Moving beyond the age-depth model paradigm in deep sea palaeoclimate archives: dual radiocarbon and stable isotope analysis on single foraminifera. Climate of the Past. 14:515–526. https://doi.org/10.5194/cp-2017-119

Lougheed BC, Obrochta SP. 2016. MatCal: Open Source Bayesian 14C Age Calibration in Matlab. Journal of Open Research Software. 4:e42. https://doi.org/10.5334/jors.130

Lougheed BC, Obrochta SP. 2019. A rapid, deterministic age-depth modelling routine for geological sequences with inherent depth uncertainty. Paleoceanography and Paleoclimatology. 34:122–133. https://doi.org/10.1029/2018PA003457

Löwemark L, Grootes PM. 2004. Large age differences between planktic foraminifers caused by abundance variations and Zoophycos bioturbation. Paleoceanography. 19(2):PA2001. https://doi.org/10.1029/2003PA000949

Löwemark L, Konstantinou KI, Steinke S. 2008. Bias in foraminiferal multispecies reconstructions of paleohydrographic conditions caused by foraminiferal abundance variations and bioturbational mixing: A model approach. Marine Geology. 256(1–4):101–106. https://doi.org/10.1016/j.margeo.2008.10.005

Metcalfe B, Lougheed BC, Waelbroeck C, Roche DM. 2020. A proxy modelling approach to assess the potential of extracting ENSO signal from tropical Pacific planktonic foraminifera. Climate of the Past. 16(3):885–910. https://doi.org/10.5194/cp-16-885-2020

Missiaen L, Wacker L, Lougheed BC, Skinner L, Hajdas I, Nouet J, Pichat S, Waelbroeck C. 2020. Radiocarbon Dating of Small-sized Foraminifer Samples: Insights into Marine sediment Mixing. Radiocarbon. 62(2):313–333. https://doi.org/10.1017/RDC.2020.13

Morard R, Quillévéré F, Escarguel G, de Garidel-Thoron T, de Vargas C, Kucera M. 2013. Ecological modeling of the temperature dependence of cryptic species of planktonic Foraminifera in the Southern Hemisphere. Palaeogeography, Palaeoclimatology, Palaeoecology. 391:13–33. https://doi.org/10.1016/j.palaeo.2013.05.011

Nayudu YR. 1964. Volcanic ash deposits in the Gulf of Alaska and problems of correlation of deep-sea ash deposits. Marine Geology. 1(3):194–212. https://doi.org/10.1016/0025-3227(64)90058-1

Parker FL, Berger WH. 1971. Faunal and solution patterns of planktonic Foraminifera in surface sediments of the South Pacific. Deep Sea Research and Oceanographic Abstracts. 18(1):73–107. https://doi.org/10.1016/0011-7471(71)90017-9

Parnell AC, Haslett J, Allen JRM, Buck CE, Huntley B. 2008. A flexible approach to assessing synchroneity of past events using Bayesian reconstructions of sedimentation history. Quaternary Science Reviews. 27(19–20):1872–1885. https://doi.org/10.1016/j.quascirev.2008.07.009

Peng T-H, Broecker WS, Berger WH. 1979. Rates of benthic mixing in deep-sea sediment as determined by radioactive tracers. Quaternary Research. 11(1):141–149.

Pisias NG. 1983. Geologic time series from deep-sea sediments: Time scales and distortion by bioturbation. Marine Geology. 51(1–2):99–113.

Reimer PJ, Austin WEN, Bard E, Bayliss A, Blackwell PG, Ramsey CB, Butzin M, Cheng H, Edwards RL, Friedrich M, et al. 2020. The IntCal20 Northern Hemisphere Radiocarbon Age Calibration Curve (0–55 Cal kBP). Radiocarbon.:1–33. https://doi.org/10.1017/RDC.2020.41

Roche DM, Waelbroeck C, Metcalfe B, Caley T. 2018. FAME (v1.0): a simple module to simulate the effect of planktonic foraminifer species-specific habitat on their oxygen isotopic content. Geoscientific Model Development. 11(9):3587–3603. https://doi.org/10.5194/gmd-11-3587-2018

Rubin M, Suess HE. 1955. U.S. Geological Survey Radiocarbon Dates 11. Science. 121:481–488.

Ruddiman WF, Glover LK. 1972. Vertical mixing of ice-rafted volcanic ash in North Atlantic sediments. Geological Society of America Bulletin. 83(9):2817–2836.

Ruddiman WF, Heezen BC. 1967. Differential solution of Planktonic Foraminifera. Deep Sea Research and Oceanographic Abstracts. 14(6):801–808. https://doi.org/10.1016/S0011-7471(67)80016-0

Schiffelbein P. 1984. Effect of benthic mixing on the information content of deep-sea stratigraphical signals. Nature. 311(5987):651. https://doi.org/10.1038/311651a0

Sepulcre S, Durand N, Bard E. 2017. Large 14C age offsets between the fine fraction and coexisting planktonic foraminifera in shallow Caribbean sediments. Quaternary Geochronology. 38:61–74. https://doi.org/10.1016/j.quageo.2016.12.002

Stuiver M, Pearson GW, Braziunas T. 1986. Radiocarbon age calibration of marine samples back to 9000 cal yr BP. Radiocarbon. 28(2B):980–1021.

Trauth MH, Sarnthein M, Arnold M. 1997. Bioturbational mixing depth and carbon flux at the seafloor. Paleoceanography. 12(3):517–526.

Waelbroeck C, Lougheed BC, Vazquez Riveiros N, Missiaen L, Pedro J, Dokken T, Hajdas I, Wacker L, Abbott P, Dumoulin J-P, et al. 2019. Consistently dated Atlantic sediment cores over the last 40 thousand years. Scientific Data. 6(1):165. https://doi.org/10.1038/s41597-019-0173-8

Wheatcroft RA. 1992. Experimental tests for particle size-dependent bioturbation in the deep ocean. Limnology and Oceanography. 37(1):90–104.

Figure 1: Comparing the new ^{14}C calibration protocol to the existing ^{14}C calibration method, in the case of samples with a mean age of 12 ka, constant species abundance and various sedimentological prior scenarios. Shown in all panels: the ground-truth age distribution (blue solid line); the age distribution estimated using the new ^{14}C calibration protocol with sedimentological priors (orange dashed line); the age distribution estimated using the traditional ^{14}C calibration method (yellow filled area). A_{det} is the expected mean ^{14}C activity determination resulting from the ground-truth age distribution according to *IntCal20*. The following scenarios are considered as sedimentological priors: Panel A: SAR 4 cm ka^{-1}, BD 10 cm; Panel B: SAR 6 cm ka^{-1}, BD 10 cm; Panel C: SAR 8 cm ka^{-1}, BD 10 cm; Panel D: SAR 10 cm ka^{-1}, BD 10 cm; Panel E: SAR 12 cm ka^{-1}, BD 10 cm; Panel F: SAR 14 cm ka^{-1}, BD 10 cm; Panel G: SAR 16 cm ka^{-1}, BD 10 cm; Panel H: SAR 18 cm ka^{-1}, BD 10 cm; Panel I: SAR 20 cm ka^{-1}, BD 10 cm;

Figure 2: Comparing the new ^{14}C calibration protocol to the existing ^{14}C calibration method, in the case of samples with a mean age of 32 ka, constant species abundance and various sedimentological prior scenarios. Shown in all panels: the ground-truth age distribution (blue solid line); the age distribution estimated using the new ^{14}C calibration protocol with sedimentological priors (orange broken line); the age distribution estimated using the traditional ^{14}C calibration method (yellow filled area). A_{det} is the expected mean ^{14}C activity determination resulting from the ground-truth age distribution according to *IntCal20*. The following scenarios are considered as sedimentological priors: Panel A: SAR 4 cm ka^{-1}, BD 10 cm; Panel B: SAR 6 cm ka^{-1}, BD 10 cm; Panel C: SAR 8 cm ka^{-1}, BD 10 cm; Panel D: SAR 10 cm ka^{-1}, BD 10 cm; Panel E: SAR 12 cm ka^{-1}, BD 10 cm; Panel F: SAR 14 cm ka^{-1}, BD 10 cm; Panel G: SAR 16 cm ka^{-1}, BD 10 cm; Panel H: SAR 18 cm ka^{-1}, BD 10 cm; Panel I: SAR 20 cm ka^{-1}, BD 10 cm;

Figure 3: Visualisation of the theoretical species abundance function used in this study to demonstrate the incorporation of prior information about species abundance in the ^{14}C calibration protocol developed in this study. The abundance function is implemented as a sine wave with a wavelength of 2000 yr.

Figure 4: Comparing the new ^{14}C calibration protocol to the existing ^{14}C calibration method, in the case of samples with a mean age of 12 ka, temporally dynamic species abundance and various sedimentological prior scenarios. Shown in all panels: the ground-truth age distribution (blue solid line); the age distribution estimated using the new ^{14}C calibration protocol with sedimentological priors (orange broken line); the age distribution estimated using the traditional ^{14}C calibration method (yellow filled area). A_{det} is the expected mean ^{14}C activity determination resulting from the ground-truth age distribution according to *IntCal20*. The following scenarios are considered as sedimentological priors: Panel A: SAR 4 cm ka^{-1}, BD 10 cm; Panel B: SAR 6 cm ka^{-1}, BD 10 cm; Panel C: SAR 8 cm ka^{-1}, BD 10 cm; Panel D: SAR 10 cm ka^{-1}, BD 10 cm; Panel E: SAR 12 cm ka^{-1}, BD 10 cm; Panel F: SAR 14 cm ka^{-1}, BD 10 cm; Panel G: SAR 16 cm ka^{-1}, BD 10 cm; Panel H: SAR 18 cm ka^{-1}, BD 10 cm; Panel I: SAR 20 cm ka^{-1}, BD 10 cm;

Figure 5: Comparing the new ^{14}C calibration protocol to the existing ^{14}C calibration method, in the case of samples with a mean age of 32 ka, temporally dynamic species abundance and various sedimentological prior scenarios. Shown in all panels: the ground-truth age distribution (blue solid line); the age distribution estimated using the new ^{14}C calibration protocol with sedimentological priors (orange broken line); the age distribution estimated using the traditional ^{14}C calibration method (yellow filled area). A_{det} is the expected mean ^{14}C activity determination resulting from the ground-truth age distribution according to *IntCal20*. The following scenarios are considered as sedimentological priors: Panel A: SAR 4 cm ka^{-1}, BD 10 cm; Panel B: SAR 6 cm ka^{-1}, BD 10 cm; Panel C: SAR 8 cm ka^{-1}, BD 10 cm; Panel D: SAR 10 cm ka^{-1}, BD 10 cm; Panel E: SAR 12 cm ka^{-1}, BD 10 cm; Panel F: SAR 14 cm ka^{-1}, BD 10 cm; Panel G: SAR 16 cm ka^{-1}, BD 10 cm; Panel H: SAR 18 cm ka^{-1}, BD 10 cm; Panel I: SAR 20 cm ka^{-1}, BD 10 cm;

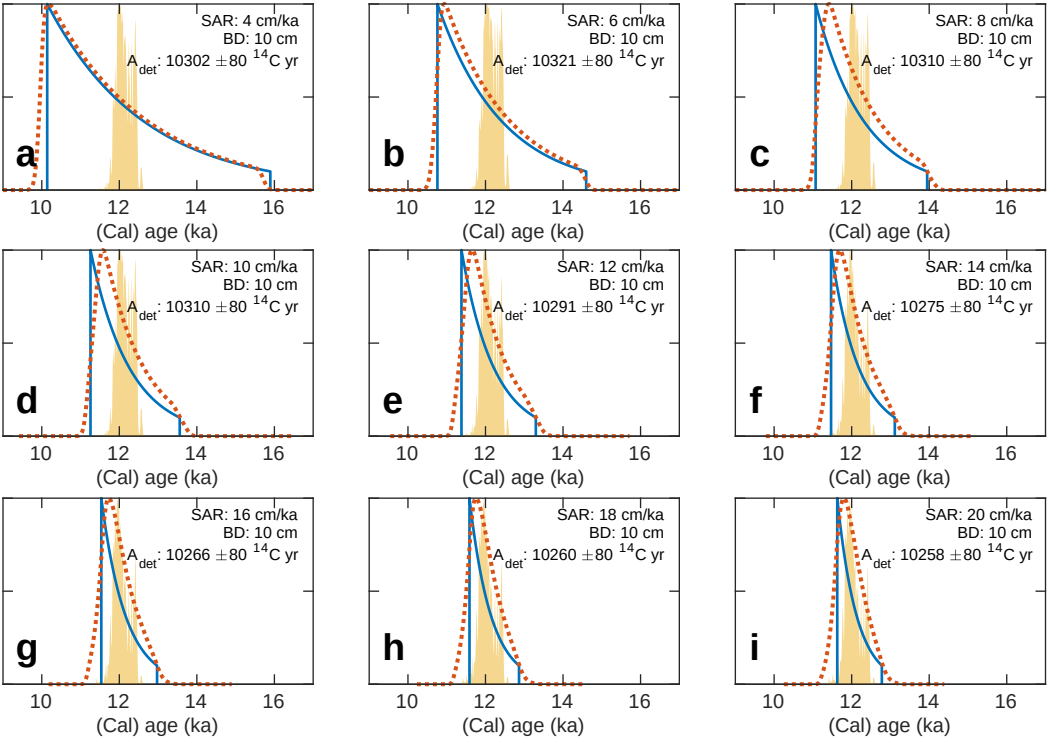
a
SAR: 4 cm/ka
BD: 10 cm
A_det: 10302 ±80 14C yr
b
SAR: 6 cm/ka
BD: 10 cm
A_det: 10321 ±80 14C yr
c
SAR: 8 cm/ka
BD: 10 cm
A_det: 10310 ±80 14C yr
d
SAR: 10 cm/ka
BD: 10 cm
A_det: 10310 ±80 14C yr
e
SAR: 12 cm/ka
BD: 10 cm
A_det: 10291 ±80 14C yr
f
SAR: 14 cm/ka
BD: 10 cm
A_det: 10275 ±80 14C yr
g
SAR: 16 cm/ka
BD: 10 cm
A_det: 10266 ±80 14C yr
h
SAR: 18 cm/ka
BD: 10 cm
A_det: 10260 ±80 14C yr
i
SAR: 20 cm/ka
BD: 10 cm
A_det: 10258 ±80 14C yr
10
12
14
16
(Cal) age (ka)

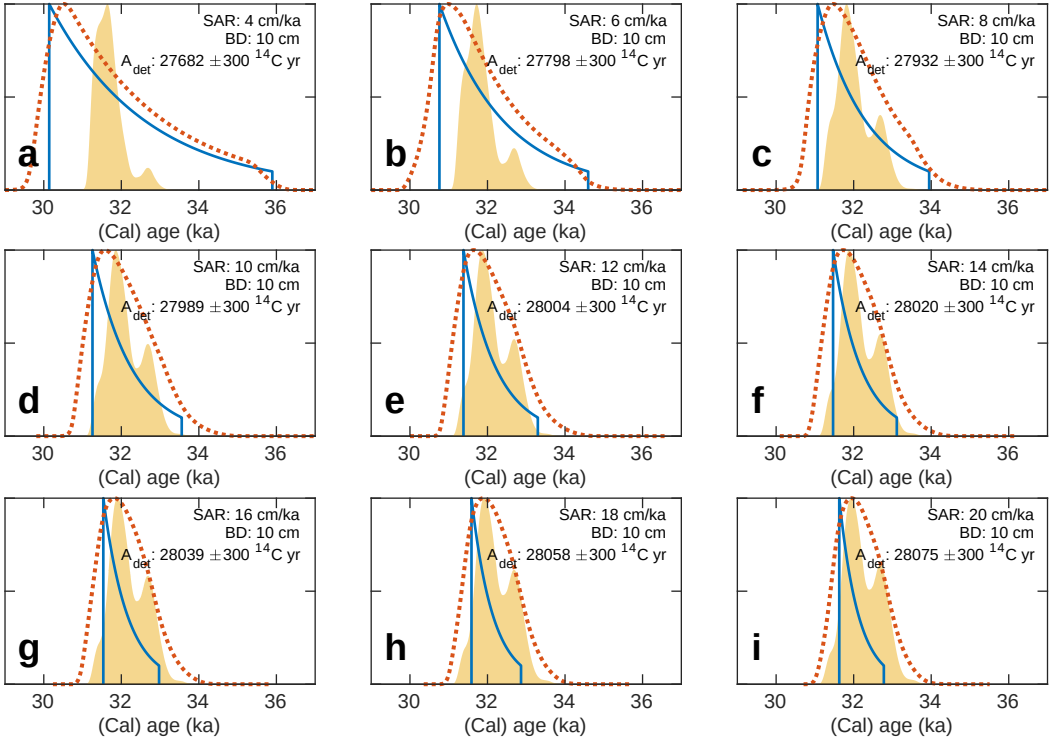
SAR: 4 cm/ka
BD: 10 cm
A det: 27682 ±300 14C yr
a
SAR: 6 cm/ka
BD: 10 cm
A det: 27798 ±300 14C yr
b
SAR: 8 cm/ka
BD: 10 cm
A det: 27932 ±300 14C yr
c
SAR: 10 cm/ka
BD: 10 cm
A det: 27989 ±300 14C yr
d
SAR: 12 cm/ka
BD: 10 cm
A det: 28004 ±300 14C yr
e
SAR: 14 cm/ka
BD: 10 cm
A det: 28020 ±300 14C yr
f
SAR: 16 cm/ka
BD: 10 cm
A det: 28039 ±300 14C yr
g
SAR: 18 cm/ka
BD: 10 cm
A det: 28058 ±300 14C yr
h
SAR: 20 cm/ka
BD: 10 cm
A det: 28075 ±300 14C yr
i
30
32
34
36
(Cal) age (ka)

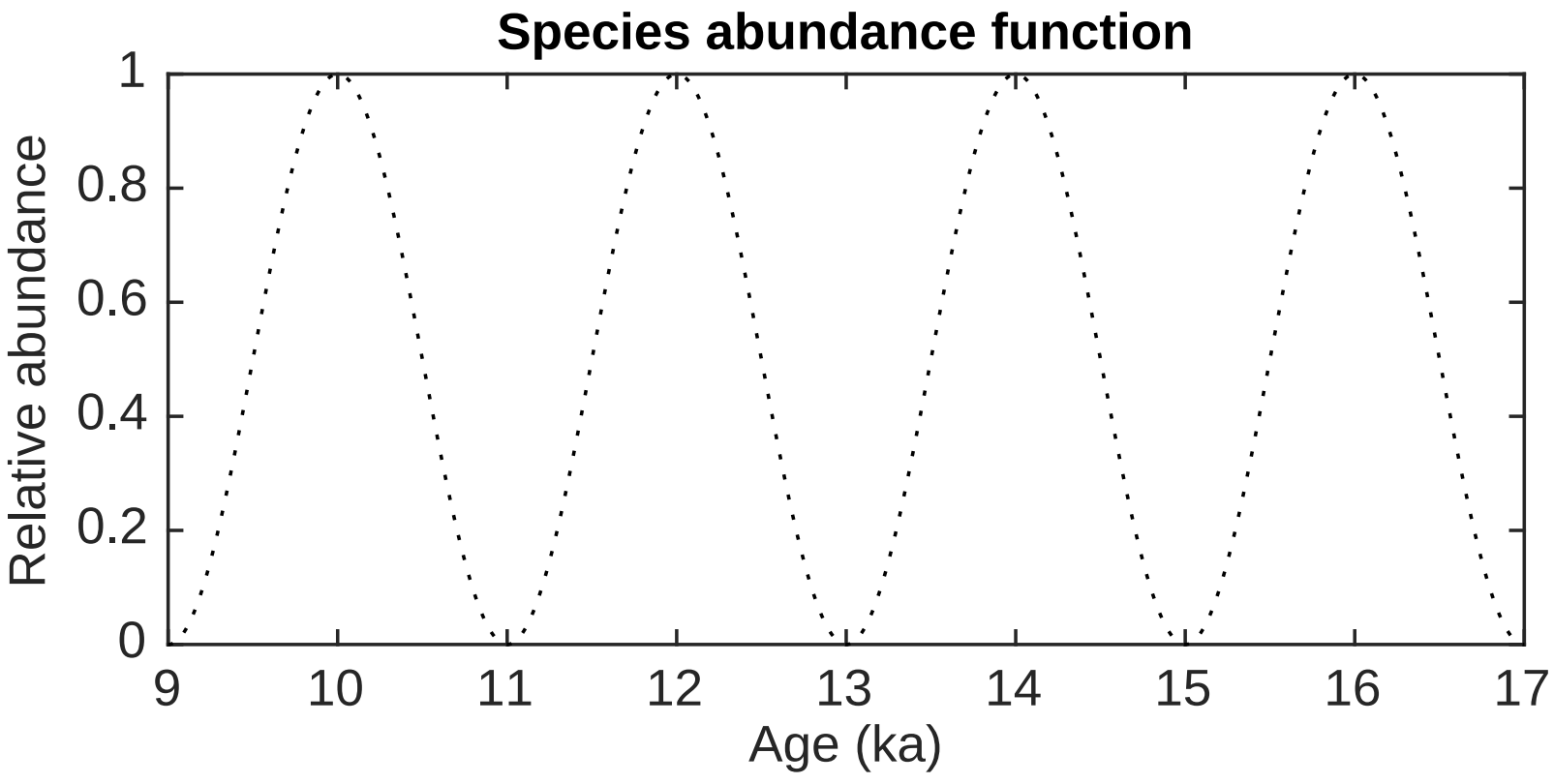
Species abundance function
Relative abundance
1
0.8
0.6
0.4
0.2
0
9
10
11
12
13
14
15
16
17
Age (ka)

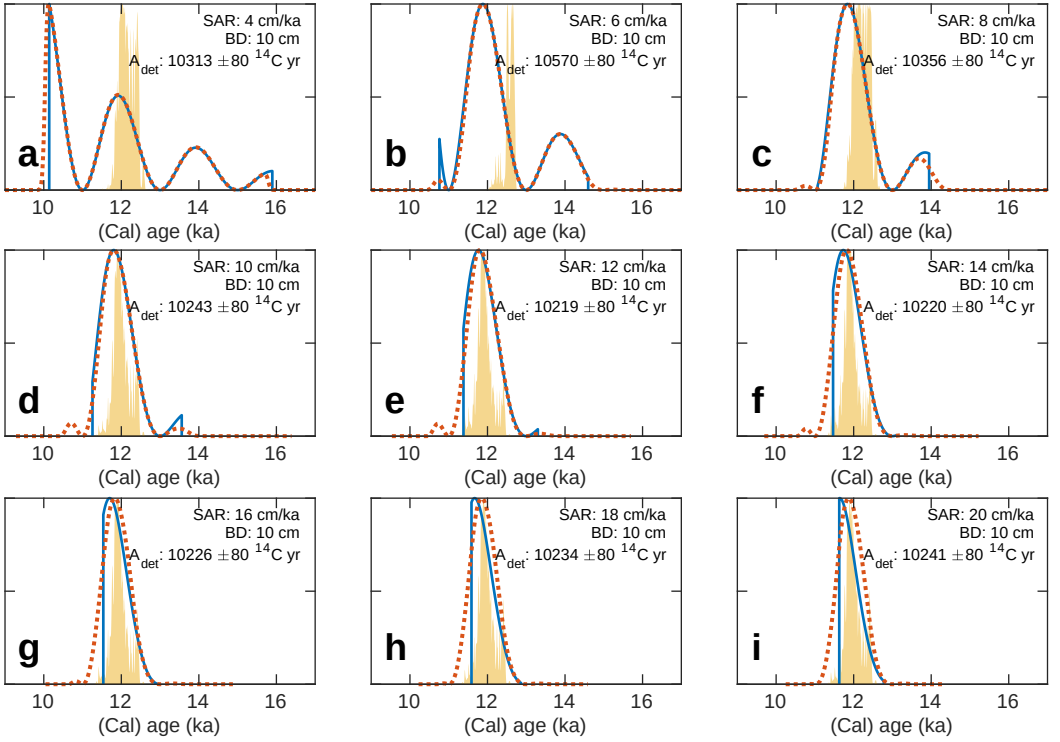
a
SAR: 4 cm/ka
BD: 10 cm
A det: 10313 ±80 14C yr
b
SAR: 6 cm/ka
BD: 10 cm
A det: 10570 ±80 14C yr
c
SAR: 8 cm/ka
BD: 10 cm
A det: 10356 ±80 14C yr
d
SAR: 10 cm/ka
BD: 10 cm
A det: 10243 ±80 14C yr
e
SAR: 12 cm/ka
BD: 10 cm
A det: 10219 ±80 14C yr
f
SAR: 14 cm/ka
BD: 10 cm
A det: 10220 ±80 14C yr
g
SAR: 16 cm/ka
BD: 10 cm
A det: 10226 ±80 14C yr
h
SAR: 18 cm/ka
BD: 10 cm
A det: 10234 ±80 14C yr
i
SAR: 20 cm/ka
BD: 10 cm
A det: 10241 ±80 14C yr
10
12
14
16
(Cal) age (ka)

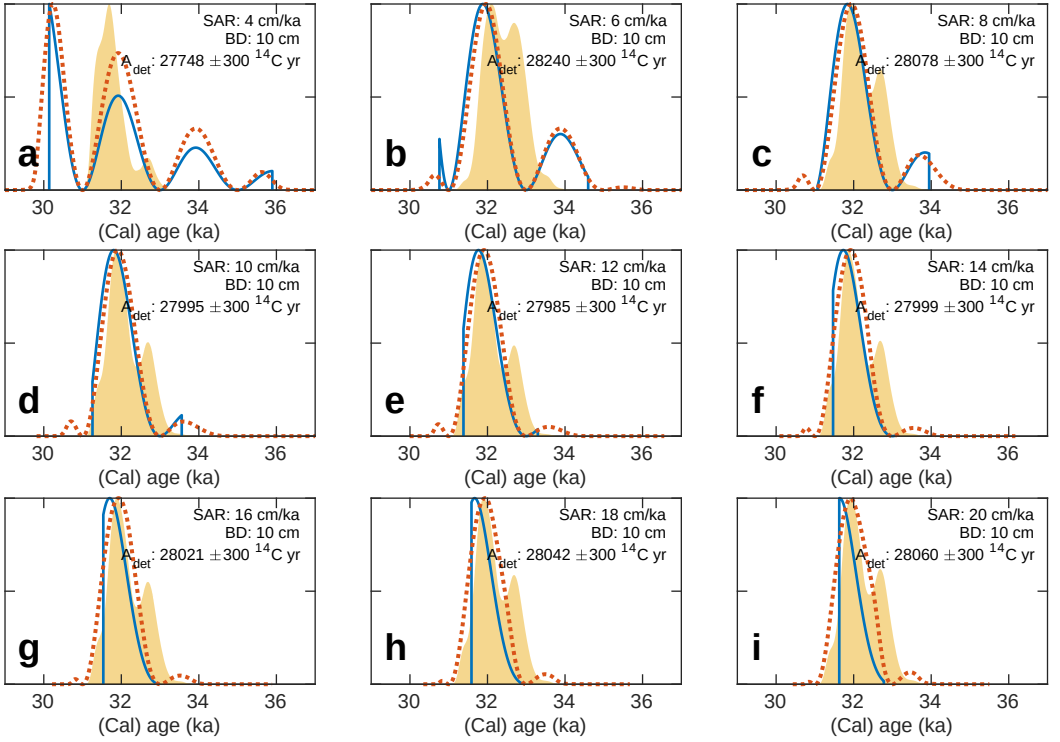
a
SAR: 4 cm/ka
BD: 10 cm
A_det: 27748 ±300 14C yr
b
SAR: 6 cm/ka
BD: 10 cm
A_det: 28240 ±300 14C yr
c
SAR: 8 cm/ka
BD: 10 cm
A_det: 28078 ±300 14C yr
d
SAR: 10 cm/ka
BD: 10 cm
A_det: 27995 ±300 14C yr
e
SAR: 12 cm/ka
BD: 10 cm
A_det: 27985 ±300 14C yr
f
SAR: 14 cm/ka
BD: 10 cm
A_det: 27999 ±300 14C yr
g
SAR: 16 cm/ka
BD: 10 cm
A_det: 28021 ±300 14C yr
h
SAR: 18 cm/ka
BD: 10 cm
A_det: 28042 ±300 14C yr
i
SAR: 20 cm/ka
BD: 10 cm
A_det: 28060 ±300 14C yr
30
32
34
36
(Cal) age (ka)